Modeling of Laser-Pumped Tm and Ho Lasers Accounting for Upconversion and Ground-State Depletion

Gunnar Rustad and Knut Stenersen

Abstract—**Models for numerical simulations of laser-pumped thulium- and thulium-holmium-doped lasers have been developed. In the models, upconversion losses and ground-state depletion in both thulium and holmium are accounted for, as well as spatial dependencies of the pump and resonator modes. The models apply to CW operation and to the build-up of population inversion prior to lasing in pulsed modes of operation. It is shown that upconversion losses in Tm:Ho:YAG significantly reduce the output from the laser in both CW and Q-switched mode. Simulations of CW lasers show good agreement with experimental results.**

I. Introduction

THULIUM- and thulium–holmium-doped laser systems are important sources for 2-μm laser radiation. This wavelength band is attractive in a number of applications, including various remote sensing applications and in medical and military technology. Following the rapid development of high-power laser-diode arrays in the past decade, thulium- and thulium–holmium-doped laser systems have gained renewed interest, owing to their potential for efficient laser-diode-pumped operation. However, efficient lasers based on these materials are difficult to design because of the quasi-three-level nature of the laser transition, where the lower laser level is thermally populated at room temperature. This results in considerable reabsorption on the laser transition and in an increased threshold for laser operation. Reducing reabsorption while maintaining efficient absorption of the pump light is one of the key issues in the design of thulium-doped laser systems.

Another problem is the low effective cross section for stimulated emission in these materials. This means that a considerable fraction of the laser ions must be excited during laser operation, which leads to a reduced absorption of pump light due to the reduced ground-state population density. Additionally, there exist upconversion (UC) processes in both thulium and holmium which reduce the population in the upper laser level under intense pumping, thereby significantly reducing the efficiency of the laser under certain operating conditions. To develop efficient lasers with these materials, it is useful to have access to accurate laser simulation models where the above mentioned effects are taken into account.

Manuscript received January 22, 1996; revised May 7, 1996. This work was supported in part by the Research Council of Norway.

The authors are with the Norwegian Defence Research Establishment, N-2007 Kjeller, Norway.

Publisher Item Identifier S 0018-9197(96)06277-X.

There are various approaches to the simulation of the behavior of these laser systems. A full rate-equation description of the populations in the many energy levels in the system is possible [1]–[3], but very calculation intensive, and spatial variation of the pump and laser beams is difficult to take into account. In other models, steady-state equations for the populations have been developed [4]–[6]. This approach is considerably less demanding on the computer power, and spatial distributions can be accounted for. However, neither UC-processes nor ground-state depletion (GSD) have been accounted for in the latter models.

In this work, a model which includes UC and GSD as well as spatial variations is developed from the rate equations for both CW and pre-pulse Q-switched operation. The effects of GSD and UC on laser performance are shown, and numerical simulations are compared with experimental results. The models are specialized to the thulium and holmium laser systems, but can be applied to other systems where similar problems occur. In our treatment of the thulium–holmium system, special attention will be directed at the distribution of the excited population between the thulium and the holmium ions as well as how this distribution is altered due to GSD in both thulium and holmium.

II. Spatial Distributions

In this work, the spatial dependence of the photon density is included by introducing the normalized photon density $\phi(x,y,z)$ (unit cm^{-3}). The photon density in the resonator is then given by $\Phi(x,y,z) = \Omega\phi(x,y,z)$ where Ω is the total photon number in the resonator. By integrating the homogeneous rate equation for the photon density over the resonator volume, a rate equation for the total photon number is obtained [4], [5]

$$\frac{d\Omega}{dt} = \int_V \left(\frac{d\Phi}{dt}\right) dV = \frac{\sigma c}{n}\int_V \Delta N(x,y,z)\Omega\phi(x,y,z)dV - \frac{\Omega}{\tau_c} \quad (1)$$

where $\Phi(x,y,z)$ is assumed independent of time (e.g., a TEM_{00} mode), $\Delta N(x,y,z)$ is the population inversion density on the laser transition, and the integration extends over the resonator volume. σ is the stimulated emission cross section for the laser transition, c is the speed of light in vacuum, n is the refractive index of the laser material, and τ_c is the cavity

lifetime (equal to the cavity round-trip time divided by the total logarithmic round-trip loss).

In steady-state laser operation, $d\Omega/dt$ equals zero, and we may write

$$\int_{V_M} \Delta N(x,y,z)\phi(x,y,z)dV = \frac{\delta}{2\sigma}\frac{n}{l_o} \tag{2}$$

where the integration extends over the volume of the laser material (since $\Delta N = 0$ outside the laser material), δ is the logarithmic round-trip loss including output coupling, and l_o is the (one way) length of the optical path in the resonator. If we assume that the laser power does not change with position along the optical axis inside the laser material (i.e., small gain), (2) can be further simplified by introducing the normalized transverse photon distribution function $\phi_r(x,y,z)$ (unit cm^{-2}). The distribution may still vary along the z axis, but the number of photons per unit length in the laser mode is independent of position along the z axis inside the laser material. We note that $\phi = \phi_r n/l_o$ inside the laser material and obtain the simple expression

$$\int_{V_M} \Delta N(x,y,z)\phi_r(x,y,z)dV = \frac{\delta}{2\sigma} \tag{3}$$

where $\phi_r(x,y,z)$ may for instance be a normalized Gaussian distribution. Together with the rate equations defined later, (1)–(3) form the basis for simulations accounting for spatial variations.

The approach outlined here requires knowledge of the resonator mode (which can be calculated from the ABCD-matrix method [7] or with optical design software). In the simulations later in this work, fundamental Gaussian resonator modes have been assumed, but simulations with other spatial distributions can easily be performed.

III. The Thulium System

The four lowest energy manifolds of trivalent thulium are sketched in Fig. 1, and the pump transition, the laser transition, and different energy transfer mechanisms are indicated. The numbering of the energy manifolds introduced here (numbered 1–4) will be used throughout this paper. The set of rate equations for the population densities in the absence of lasing is

$$\frac{dN_4}{dt} = R_4 - k_{4212}N_4N_1 + k_{2124}N_2^2 - \frac{N_4}{\tau_4} \tag{4}$$

$$\frac{dN_3}{dt} = k_{2123}N_2^2 - k_{3212}N_3N_1 + \beta_{43}\frac{N_4}{\tau_4} - \frac{N_3}{\tau_3} \tag{5}$$

$$\frac{dN_2}{dt} = 2k_{4212}N_4N_1 + 2k_{3212}N_3N_1 - 2(k_{2123}+k_{2124})N_2^2 - \frac{N_2}{\tau_2} + \beta_{32}\frac{N_3}{\tau_3} + \beta_{42}\frac{N_4}{\tau_4} \tag{6}$$

$$N_1 = N_{\text{Tm}} - \sum_{i=2}^{4} N_i \tag{7}$$

where terms accounting for stimulated emission have been omitted. R_4 is the pump rate per volume unit from level 1 into level 4, τ_i is the lifetime of level i due to spontaneous decay, β_{ij} is the branching ratio of the spontaneous transition $i \rightarrow j$, N_{Tm} is the thulium dopant concentration, and the terms for energy transfer, k_{ijkl}, describe the energy transfer processes $i \rightarrow j$ & $k \rightarrow l$.

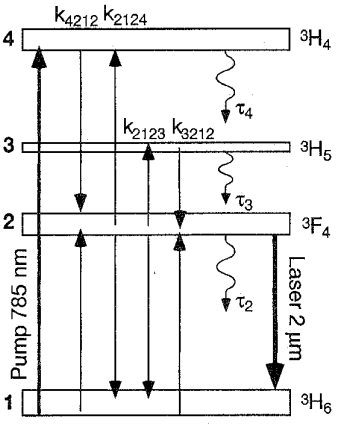

Fig. 1. Schematic view of the four lowest energy manifolds in trivalent thulium with the energy transfer mechanisms (between two thulium ions) regarded in this paper indicated.

Manifold 4 ($^3H_4$) is de-excited by spontaneous emission and the cross-relaxation process. The effective lifetime of this manifold varies with thulium dopant concentration and is for standard dopant concentrations (above 3%–4%) on the order of a few tens of microseconds in YAG [8], [9]. τ_3 has been found to be $\sim$8 μs in Tm:YAG.[1] The differential equations (4)–(5) for these manifolds can therefore be replaced by steady-state equations, taking into account the long lifetime in manifold 2, which is on the order of 10 ms in many host materials. For the same reason, it is reasonable to assume that $N_2 \gg N_3$, N_4 leading to $N_1 \approx N_{\text{Tm}} - N_2$. With these simplifications, the rate equation for the upper laser level in the thulium laser is

$$\frac{dN_2}{dt} = R_4(2\eta_4 + (1-\eta_4)(\beta_4 + \beta_{43}\eta_3)) - \frac{N_2}{\tau_2} - k_{\Sigma\text{Tm}}N_2^2 \tag{8}$$

$$k_{\Sigma\text{Tm}} = k_{2123}(1-\eta_3) + (2-\beta_4-\beta_{43}\eta_3)(1-\eta_4)k_{2124} \tag{9}$$

where $\beta_4 = \beta_{42} + \beta_{43}$, and where it has been assumed that $\beta_{32} = 1$, which is a reasonable assumption [10]. η_4 is the cross-relaxation efficiency; the fraction of ions excited to manifold 4 that is de-excited through cross-relaxation

$$\eta_4 = \frac{k_{4212}N_1\tau_4}{1 + k_{4212}N_1\tau_4}. \tag{10}$$

A similar expression defines the cross-relaxation efficiency η_3 from manifold 3 (where the indexes "4" have been replaced with "3"). The last term in (8) describes the total UC losses in the thulium laser, and $k_{\Sigma\text{Tm}}$ is the total UC loss constant.

[1] Caird *et al.* [10] calculated several of the nonradiative decay rates in Tm:YAG assuming that the energy gaps between the manifolds were equal to those of Tm:$YAlO_3$. Inserting the measured energy gaps of Tm:YAG from [11] in the calculations, all calculated nonradiative decay rates increase. For example: The nonradiative lifetime of level 3 (τ_3) decreases from 13 μs to 7.6 μs with the measured energy gaps inserted, the level 4→ 3 branching ratio (β_{43}) increases from 0.48 to 0.56, and the total level 4→ 2 branching ratio (β_4) increases from 0. 54 to 0. 61.

If the ground-state is depleted, the absorption coefficient (and normally the pump rate) is reduced according to

$$\alpha = \sigma_{\rm abs}(N_{\rm Tm} - N_2) = \alpha_0(1 - N_2/N_{\rm Tm}) \qquad (11)$$

where α_0 is the small-signal pump absorption coefficient, and $\sigma_{\rm abs}$ is the effective absorption cross section on the pump transition. Including terms for stimulated emission, we can now write the complete rate equation for the upper laser level

$$\frac{dN_2}{dt} = R_2^0\left(1 - \frac{N_2}{N_{\rm Tm}}\right) - \frac{N_2}{\tau_2} - k_{\Sigma{\rm Tm}}N_2^2 - \sigma c((f_u + f_l)N_2 - f_l N_{\rm Tm})\Phi \qquad (12)$$

where R_2^0 is the undepleted pump rate into manifold 2

$$R_2^0 = R_4^0(2\eta_4 + (1 - \eta_4)(\beta_4 + \beta_{43}\eta_3)) \qquad (13)$$

where R_4^0 is calculated with α_0. f_u and f_l are the Boltzmann thermal occupation factors of the upper and lower laser level (Stark sublevels), respectively. To account for the spatial distribution of N_2, (11)–(12) require the pump distribution to be given. This distribution will in practice be altered by GSD which reduces the pump absorption coefficient. This is particularly important in end-pumped geometries where substantial differences from the small-signal pump distribution can occur under intense pumping and nonlasing conditions. The pump distribution can be calculated numerically from (12) and

$$\frac{di_p}{dz} = -\alpha_0\left(1 - \frac{N_2}{N_{\rm Tm}}\right)i_p \qquad (14)$$

where i_p is the pump intensity. In dynamic systems where the upper level population is changing with time, e.g., in the pump interval before a Q-switched pulse, split-step numerical calculations are required.

Of the two UC processes, each UC event to the $^3H_5$ level results in an effective loss of $(1 - \eta_3)$ excited ions in the upper laser level, whereas each UC event to the $^3H_4$ level represents a loss of $(2 - \beta_4 - \beta_{43}\eta_3)(1 - \eta_4)$ upper laser level ions. $(1 - \eta_4)$ is the fraction of the ions in the $^3H_4$ level that decay spontaneously, and each ion lost through this channel represents a loss of two ions in the upper laser level, except the fraction $\beta_4 + \beta_{43}\eta_3$ which ends up in level 2 and therefore represents a loss of one ion in the upper laser level. This fraction consists of the part $\beta_{42} + \beta_{43}(1 - \eta_3)$ which represents spontaneous decay into level 2, and $2\beta_{43}\eta_3$ which represents the cross-relaxation process between levels 3 and 1, giving two ions in level 2. In Tm:YAG, each UC process to the $^3H_4$ level represents a loss of less than 0.1 excitations for dopant concentrations above 3–4% since the cross-relaxation efficiency η_4 >95% for these concentrations [8], [9], and the value of β_4 is approximately 0.6 [10]. The value of η_3 is uncertain, but is probably close to zero. This assumption is based on the fact that $\tau_3 \ll \tau_4$ ($\sim$10 μs versus $\sim$1 ms [8]–[10]) and that k_{3212}, although not measured, most likely is smaller than k_{4212} due to the larger energy deficiency of the first process.

There exist only a few published values for the UC rate constants k_{2123} and k_{2124} in Tm:YAG in the literature, and a few for the total UC loss rate, $k_{\Sigma{\rm Tm}}$. These values have been summarized in Table I for 6% Tm:YAG. Shaw *et al.* [12] found the UC rate to depend strongly on the dopant concentration according to

$$k_{ijkl} = \frac{C^2}{C^2 + C_0^2}\frac{2U_{ijkl}}{N_{100\%}} \qquad (15)$$

where C is the dopant concentration, C_0 is a characteristic dopant concentration, $N_{100\%}$ is the density of available sites in the host material, and U_{ijkl} is the UC rate for the $ijkl$ transition between ions at nearest neighbors positions in the host lattice. C_0 was found to be 4.3% for Tm:YAG, which indicates that the UC rate will be reduced by $\sim$30% if the dopant concentration is reduced from 6% to 4% of thulium in YAG.

TABLE I
SUMMARY OF PUBLISHED VALUES OF THE UC PARAMETERS IN 6% Tm:YAG

Description		(10^{-18} cm^3/s)	Reference
UC from $^3F_4$ to $^3H_4$ in Tm	k_{2124}	1-8	[12], [13]
UC from $^3F_4$ to $^3H_5$ in Tm	k_{2123}	3	[12]
UC from $^3F_4$ in Tm	$k_{\Sigma Tm}$	1.2-3.5	[14]-[16]
Calculated $k_{\Sigma Tm}$ from k_{2124} and k_{2123}	$k_{\Sigma Tm}$	3-3.4	

In calculation of $k_{\Sigma{\rm Tm}}$, parameter values listed in Table II were used.

The values in Table I are all considerably smaller than the UC rate constants in the codoped Tm:Ho:YAG laser material, where comparable rates are approximately an order of magnitude larger. However, they are still large enough to cause an observable reduction in output from a thulium laser under certain operating conditions, as shall be seen later.

A. CW Operation

In CW operation, the population inversion is saturated so that the effective round-trip gain equals the round-trip losses. Solving (12) in the steady-state case yields

$$\frac{N_2}{N_{\rm Tm}} = \frac{\sqrt{(1+i_r+I_R)^2 + 2\kappa_{\rm Tm}(i_r + fI_R)} - (1+i_r+I_R)}{\kappa_{\rm Tm}} \qquad (16)$$

where

$$f = \frac{f_l}{f_u + f_l} \qquad (17)$$

is the fraction of ions needed to be excited to level 2 to obtain optical transparency on the laser transition. In (16), the relative laser intensity has been defined as

$$I_R = I/I_{\rm sat} = h\nu_L c\Phi/I_{\rm sat} \qquad (18)$$

$$I_{\rm sat} = \frac{h\nu_L}{(f_u + f_l)\sigma\tau_2} \qquad (19)$$

and the relative pump intensity has been introduced as

$$i_r = i_p/i_p^{\rm sat} \qquad (20)$$

$$i_p^{\rm sat} = \frac{h\nu_p}{(2\eta_4 + (1 - \eta_4)(\beta_4 + \beta_{43}\eta_3))\sigma_{\rm abs}\tau_2} \qquad (21)$$

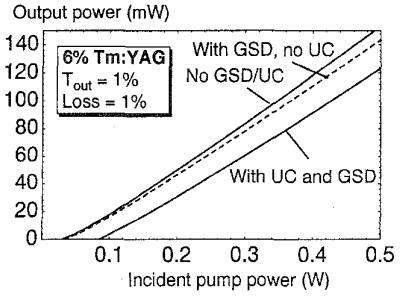

Fig. 2. Comparison of simulations of a CW end-pumped Tm:YAG laser with and without GSD and UC. The pump and resonator modes are both assumed to have overlapping Gaussian transverse distributions with 60-μm constant beam radii through the entire length of the gain medium. Simulations are according to (3) and (24), (23), or (16) (top to bottom, respectively). In the lower graph, $k_{\Sigma\mathrm{Tm}} = 3{\cdot}10^{-18}$ cm^3/s was assumed. T_{out}: Output coupling. Loss: Resonator round-trip losses (without output coupling).

where $h\nu_L$ and $h\nu_p$ are the laser and pump photon energy, respectively. The UC losses have been accounted for in

$$\kappa_{\mathrm{Tm}} = 2N_{\mathrm{Tm}}\tau_2 k_{\Sigma\mathrm{Tm}} \tag{22}$$

where $k_{\Sigma\mathrm{Tm}}$ was defined in (9). In the limit of no UC ($\kappa_{\mathrm{Tm}} \to 0$), (16) simplifies to

$$\frac{N_2}{N_{\mathrm{Tm}}} = \frac{i_r + fI_R}{1 + i_r + I_R}. \tag{23}$$

The appearance of i_r in the denominator in (23) stems from accounting for GSD. If GSD is left out from the calculations, then the common expression for saturation of the upper laser level population appears as

$$\frac{N_2}{N_{\mathrm{Tm}}} = \frac{i_r + fI_R}{1 + I_R}. \tag{24}$$

To calculate the output from a CW thulium laser, the expression for the upper laser level population density (16) is inserted into (3), and the circulating intensity I_R that satisfies the new expression is found. In Fig. 2, results from simulations with (16), (23), and (24) are compared to show the effect of UC and pump depletion in CW end-pumped thulium lasers. The parameters used in this work are listed in Table II. We see that simulations based on (24) give both a too high slope efficiency and a too low pump threshold value. The reduced slope efficiency is mainly due to the reduced pump absorption efficiency caused by GSD. The UC losses mainly contribute to a higher threshold value.

B. Q-Switched Operation

In Q-switched operation, the stimulated emission term can be neglected during pumping. Equation (12) can then be solved to yield

$$\frac{N_2(t)}{N_{\mathrm{Tm}}} = \frac{s \cdot \tanh\left(\frac{s\,t}{2\tau_2} + \operatorname{arctanh}\left(\frac{1+i_r}{s}\right)\right) - (1 + i_r)}{\kappa_{\mathrm{Tm}}} \tag{25}$$

where we have introduced

$$s = \sqrt{(1 + i_r)^2 + 2\kappa_{\mathrm{Tm}} \cdot i_r}\ . \tag{26}$$

These expressions can be used to calculate the population inversion distribution before the Q-switched pulse.

TABLE II
LIST OF PARAMETER VALUES USED IN THE SIMULATIONS UNLESS OTHERWISE STATED

Description, *symbol* [unit]	Tm: YAG	Tm:Ho: YAG	Tm:Ho: YLF
Thulium dopant concentration	6%	6%	6%
Holmium dopant concentration	-	0.5%	0.5%
$r_{HT} = N_{Ho}/N_{Tm}$	-	0.083	0.083
Length of material, l [cm]	0.5	0.5	0.5
Upper level lifetime, τ_2 [ms]	12	-	-
Combined u. level lifetime, τ [ms]	-	9	15
Stim. em. cross-section, σ [10^{-20} cm^2]	0.5	10	15
Eff. pump abs. cross-section, σ_{abs} [10^{-20} cm^2]	0.65	0.65	0.65
Refractive index, n	1.82	1.82	1.48
Temperature, T [K]	300	300	300
Boltzmann factor u. level , f_u	0.46	0.11	0.09
Boltzmann factor l. level , f_l	0.017	0.017	0.028
Tm-Ho equilibrium constant, θ	-	11	15
Beam radius inside rod, ω [μm]	60	60	60
Total branching ratio 4 → 2, β_4	0.6	0.6	0.6
Total branching ratio 8 → 6, β_8	-	1	1
Level 3 cross-rel. efficiency, η_3	0	0	0
Level 4 cross-rel. efficiency, η_4	0.97	0.97	0.97
Level 8 cross-rel. efficiency, η_8	0	0	0

Populations change due to UC and pumping will be negligible during the Q-switched pulse, and, consequently, simulations of Q-switched operation can be performed in a normal manner based on the calculated distribution prior to Q-switching. Spatial effects can be included by using split-step calculations accounting for diffraction and gain [17].

In Fig. 3, the effects of UC and GSD in Tm:YAG are shown when calculations with and without UC and GSD are compared. In the calculations, a constant relative pump intensity $i_r = 1$ has been assumed, and different values of the UC parameter that span the range of published values for Tm:YAG have been used. The time scale of the simulations is up to 20% of the upper laser level lifetime. In Tm:YAG, this corresponds to a pump pulse length of $\sim$2 ms and a pump intensity $i_p \approx 600$ W/cm^2. This is a typical value for local pump intensities in a transversal pumping geometry with quasi-CW high-power laser-diode arrays [18]. (Numerical simulation of this system requires, however, integration over the spatial pump intensity profile). For longer pump intervals or higher pump intensities, the effects of UC will be even larger.

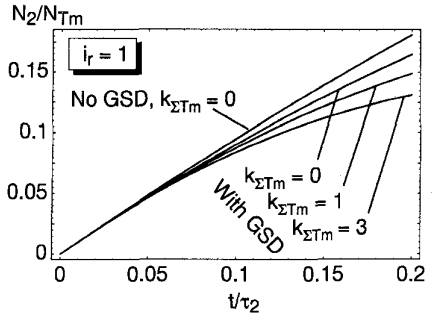

Fig. 3. Comparison of simulations with no UC or GSD, and with GSD and various UC parameters. The symbols are defined in the text. $k_{\Sigma \mathrm{Tm}}$ is given in units of 10^{-18} cm^3/s.

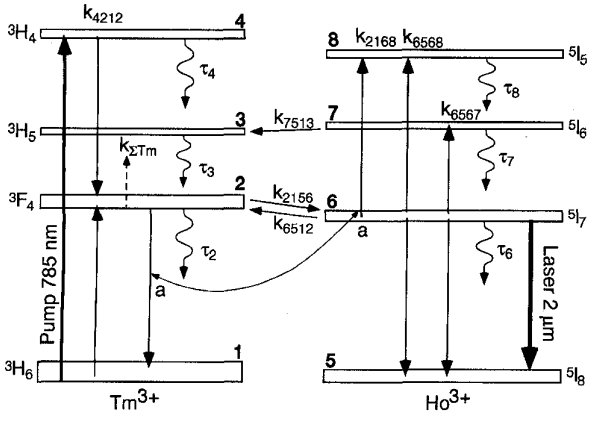

Fig. 4. Schematic view of the lower energy manifolds and atomic transitions in co-doped Tm-Ho materials. Horizontal arrows indicate energy transfer processes in which the donor is de-excited from the indicated level to the ground-state, and the acceptor is excited from the ground-state to the indicate state. The processes referred to in the text as k_{8612} and k_{8656} are the reverse of the processes k_{2168} and k_{6568} in the figure, respectively. The dashed arrow labeled $k_{\Sigma \mathrm{Tm}}$ indicates the UC processes in thulium as shown in Fig. 1.

IV. The Thulium-Holmium System

In thulium–holmium-doped laser materials, the absorption of the pump light in thulium is followed by thulium cross-relaxation and energy-transfer from the ^{3}H$_4$ level in thulium to the ^{5}I$_7$ level in holmium, which is the upper laser level. A schematic illustration of the thulium–holmium system in shown in Fig. 4. In simulations of this system, one must also take into account that energy can be transferred from holmium to thulium ions (back-transfer) and that there are UC processes in both thulium and holmium besides a strong cooperative UC process where one holmium ion is excited and one thulium ion is de-excited (process a in Fig. 4).

The UC processes from the ^{5}I$_7$ level in holmium have terminal levels ^{5}I$_5$ and ^{5}I$_6$, marked with k_{6568} and k_{6567}, respectively, in Fig. 4. In the cooperative UC process, (k_{2168}), a holmium ion in the upper laser level, is excited to the ^{5}I$_5$ level while a thulium ion in the ^{3}F$_4$ level is de-excited. From the ^{5}I$_5$ level, the energy can either rapidly decay to the ^{5}I$_6$ level or cross-relax back to the upper laser level in holmium (cross-relaxation processes k_{8656} and k_{8612} are not shown in Fig. 4, but are the reverse of the UC processes marked k_{6568} and k_{2168}, respectively). From the ^{5}I$_6$ level, the energy can either decay to the ^{5}I$_7$ level or be transferred to the thulium ^{3}H$_5$ level, followed by rapid nonradiative decay to the thulium ^{3}F$_4$ level [3], [10], [19].

Of the UC processes described above, the cooperative process, including a thulium ion in the ^{3}F$_4$ level and a holmium ion in the ^{5}I$_7$ level (k_{2168}), is by far the most important loss process compared to the holmium-holmium UC processes (k_{6567} and k_{6568}). The average interaction distance in the energy transfer processes will be close to the shortest ion-ion distance in migration-assisted energy transfer since the transfer probability is inversely dependant on the distance in the sixth power [20]. Typically, the ratio of the dopant concentrations is approximately 10:1 (Tm:Ho). The distance between the thulium ions and between thulium and holmium ions will then be considerably shorter (both the average distance and the density of ions at nearest neighbor positions in the host lattice) than the distance between the holmium ions. It is therefore reasonable to assume that the holmium-holmium UC will be significantly less important than the cooperative UC (k_{2168}). This has also been confirmed in measurements (see Table III). We shall, therefore, in the following ignore the holmium UC processes, marked with k_{6567} and k_{6568} in Fig. 4. Additionally, there exist other processes (both excited-state-absorption and cooperative UC ^{3}H$_4 \rightarrow {}^3$H$_6$; ^{5}I$_7 \rightarrow {}^3$F$_4$ or ^{5}S$_2$) in thulium–holmium doped materials which lead to visible emission from the laser crystal, but these are considered to be much weaker than the processes described above [3], and we have therefore chosen to disregard these processes. With the above assumptions, the rate equations for the thulium ^{3}F$_4$ level and the holmium ^{5}I$_7$ level can be written as

$$\begin{aligned}\dot{N}_2 = {} & R_2^0\left(1-\frac{N_2}{N_{\mathrm{Tm}}}\right)-\frac{N_2}{\tau_2}-k_{\Sigma\mathrm{Tm}}N_2^2 \\ & -k_{2156}N_2N_5+k_{1265}N_1N_6 \\ & -k_{2168}N_2N_6(1-\eta_7(1-\eta_8)(1+\eta_3)\beta_{87}-\eta_{8(2)})\end{aligned} \tag{27}$$

$$\begin{aligned}\dot{N}_6 = {} & k_{2156}N_2N_5-k_{1265}N_1N_6-\frac{N_6}{\tau_6} \\ & -k_{2168}N_2N_6 \\ & \times(1-(1-\eta_8)(\beta_{86}+(1-\eta_8)\beta_{87}\beta_{76})-2\eta_{8(6)}-\eta_{8(2)})\end{aligned} \tag{28}$$

where $N_1 \approx N_{\mathrm{Tm}} - N_2$ and $N_5 \approx N_{\mathrm{Ho}} - N_6$, and β_{ij} denotes the branching ratio for the spontaneous transition $i \rightarrow j$. Cross-relaxation from level 8 includes the processes k_{8612} and k_{8656}. We have here defined the cross-relaxation efficiency η_8 in a similar manner to that of level 4 in (10) where both cross-relaxation processes have been included, written as

$$\eta_8 = \frac{k_{8612}N_1 + k_{8656}N_5}{k_{8612}N_1 + k_{8656}N_5 + 1/\tau_8}. \tag{29}$$

For notational convenience, we have also defined the cross-relaxation efficiencies to levels 2 and 6, $\eta_{8(2)}$ and $\eta_{8(6)}$, respectively, as the ratio of the first (the second for $\eta_{8(6)}$) term in the numerator in (29) to the denominator. In (27), an "energy-transfer efficiency" from level 7 (η_7) has been defined as the ratio of the rate of decay from level 7 due to energy transfer to level 3 to the total decay rate of level

TABLE III
SUMMARY OF PUBLISHED VALUES OF THE UC CONSTANTS IN Tm:Ho-DOPED YAG and YLF

Material	Author	Measured UC const.	k_{2168}	$k_{\Sigma Ho}$
6%Tm,	Antipenko [32]	$k = 80$	80	20
0.5%Ho:YAG	Armagan [13]	$p_{27} = 20$	[a]	[a]
	Bowman [21]	$q = 140$	72	18
	Fan [19]	$q = 24$	12	3
	Kintz [30]	$q = 30$	15	3.7
	Nikitichev [25]	$k = 80$	80	20
6%Tm,	Dinndorf [33]	$\alpha_2 = 15$	15	3.7
0.5%Ho:YLF	Hansson [31]	$q = 5$	2.5	0.6
2.0% Ho:YAG	Antipenko [32]	$k_{6568} + k_{6567} < 0.8$		
0.5% Ho:YAG	Shaw [12]	$k_{6568} \approx 0$, $k_{6567} < 0.2$		

The Ho UC values have been deduced from measurements on higher holmium dopant concentrations. All units are in 10^{-18}cm^3/s.

[a] Insufficient information in the paper to calculate k_{2168} and $k_{\Sigma \mathrm{Ho}}$.

7. Measurements of the cross-relaxation process from level 7, k_{7656}, indicate that this rate is very slow compared to the other rates in the system [12]. This rate has therefore been neglected in the deduction of (27)–(28).

The migration-assisted energy transfer from the thulium $^3F_4$ level to the holmium $^5I_7$ level and the back-transfer from holmium to thulium cause an equilibrium between the population densities in thulium and holmium in steady-state operation. The average transfer time between thulium and holmium is in the range of 10 μs in YAG and YLF with normal dopant concentrations (4–6%Tm, 0.5%Ho) [9], [19], [21]–[23]. This is fast enough for the equilibrium to be only slightly altered under CW and free-running pulsed laser operating conditions, but slow compared to typical time scales in Q-switched operation. A result of the latter fact is that only the energy stored in holmium prior to a Q-switched pulse can be extracted during the pulse, which leads to a significant limitation in overall efficiency in Q-switched thulium–holmium lasers.

To calculate the gain in the thulium–holmium laser, we need to find the fraction of the excitations that are stored in holmium ions. This can be done if we assume that the energy transfer rate is considerably larger than any other rate in the rate equations, which is the case in CW and free-running laser operation. Steady state then occurs when the forward-transfer and back-transfer rates are equal, as

$$k_{2156} N_2 N_5 = k_{1265} N_1 N_6. \tag{30}$$

Defining a constant θ as the ratio of the energy transfer parameters, we find

$$\theta = \frac{k_{2156}}{k_{1265}} = \frac{N_6}{N_2} \cdot \frac{N_{\mathrm{Tm}}(1 - N_2/N_{\mathrm{Tm}})}{N_{\mathrm{Ho}}(1 - N_6/N_{\mathrm{Ho}})}. \tag{31}$$

Traditionally, the distribution of population between thulium and holmium has been assumed to follow that of a Boltzmann distribution weighted with the dopant concentrations [24]. In this approach, the value of θ is simply the ratio of the partition functions of the $^5I_7$ and $^3F_4$ manifolds

$$\theta = \frac{\sum_{i \in {}^5\mathrm{I}_7} g_i e^{-E_i/k_B T}}{\sum_{j \in {}^3\mathrm{F}_4} g_j e^{-E_j/k_B T}} \tag{32}$$

where the summation extends over the Stark levels in the respective manifolds, k_B is the Boltzmann constant, T is the temperature, and g_i is the degeneracy of level i. However, recent works have shown that the distribution of energy levels in the ground states of thulium and holmium should also be accounted for in calculation of the constant θ [25], [26]

$$\theta = \frac{\sum_{i \in {}^5\mathrm{I}_7} g_i e^{-E_i/k_B T}}{\sum_{j \in {}^3\mathrm{F}_4} g_j e^{-E_j/k_B T}} \cdot \frac{\sum_{k \in {}^3\mathrm{H}_6} g_k e^{-E_k/k_B T}}{\sum_{l \in {}^5\mathrm{I}_g} g_l e^{-E_l/k_B T}}. \tag{33}$$

At room temperature, the constant θ is 11 in YAG and 15 in YLF, in contrast to 21 and 26, respectively, from calculations based on (32) [11], [27]–[29]. The consequences of this are that less energy is stored in holmium than previously believed, as is illustrated in Fig. 5. From (31), an expression for the fraction of the excited population that is stored in the upper laser level in the holmium ions can be found: $(N_x = N_2 + N_6)$

$$\begin{aligned} f_{\mathrm{Ho}} &= \frac{N_6}{N_x} \\ &= \frac{1}{2} + \frac{1 + \theta r_{\mathrm{HT}}}{2(\theta - 1) n_x} \\ &\quad - \frac{\sqrt{(1 + \theta r_{\mathrm{HT}} + (\theta - 1) n_x)^2 - 4(\theta - 1) n_x \theta r_{\mathrm{HT}}}}{2(\theta - 1) n_x} \end{aligned} \tag{34}$$

where $n_x = N_x/N_{\mathrm{Tm}}$ and $r_{\mathrm{HT}} = N_{\mathrm{Ho}}/N_{\mathrm{Tm}}$. This is illustrated in Fig. 5, where f_{Ho} and N_6 are plotted as a function of N_x for $\theta = 11$ and 21 (new and old values of θ in Tm:Ho:YAG). We see that the fractional population in holmium is reduced at higher excitation levels. This stems from depletion of the holmium ground-state; a reduced acceptor density leads to a reduced transfer rate, which leads to a displacement of the equilibrium toward thulium.

In the limit of no excited population, $(n_x \to 0)$, f_{Ho} approaches the small-signal value

$$f^0_{\mathrm{Ho}} = \frac{r_{\mathrm{HT}} \theta}{1 + r_{\mathrm{HT}} \theta}. \tag{35}$$

When the levels 2 and 6 are at equilibrium, their rate equations (27) can be combined to yield a rate equation for the total excited population density in the system consisting of the two upper levels

$$\begin{aligned} \frac{dN_x}{dt} &= R^0_2 \left(1 - (1 - f_{\mathrm{Ho}}) \frac{N_x}{N_{\mathrm{Tm}}}\right) - \frac{N_x}{\tau} - k_{\Sigma \mathrm{Ho}} N_x^2 \\ &\quad - \sigma c (f_{\mathrm{Ho}}(f_u + f_l) N_x - f_l N_{\mathrm{Ho}}) \Phi \end{aligned} \tag{36}$$

$$\begin{aligned} k_{\Sigma \mathrm{Ho}} &= k_{\Sigma \mathrm{Tm}} (1 - f_{\mathrm{Ho}})^2 + (1 - \eta_8) \\ &\quad \times (2 - \beta_8 - \eta_7 \beta_{87} (\beta_{75} + \eta_3)) k_{2168} f_{\mathrm{Ho}} (1 - f_{\mathrm{Ho}}) \end{aligned} \tag{37}$$

where f_u and f_l are the Boltzmann thermal occupation factors for the upper and lower laser level relative to the total

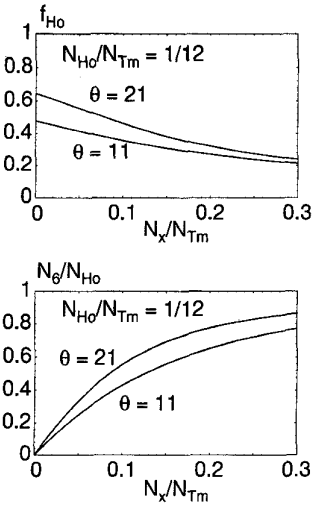

Fig. 5. Illustration of how the equilibrium between the upper level populations in thulium and holmium is displaced toward thulium at greater excitation densities. The two values of θ correspond to the two different approaches to calculate θ in the literature.

population in the upper and lower holmium energy manifolds, respectively. σ is the cross section for stimulated emission in holmium, $\beta_8 = \beta_{86} + \beta_{87}\beta_{76}$ is the total branching ratio from level 8 to level 6, and we have used $\eta_{8(2)} + \eta_{8(6)} = \eta_8$. The rate for spontaneous emission from the combined levels, $1/\tau$, is introduced as

$$\frac{1}{\tau} = \frac{1 - f_{\mathrm{Ho}}}{\tau_2} + \frac{f_{\mathrm{Ho}}}{\tau_6}. \tag{38}$$

Equations (36)–(37) can be used for numerical simulations of the thulium–holmium laser system. In the steady-state case, a fourth-degree equation is obtained for N_x when (34) is inserted into (36). This can be solved analytically if the term regarding UC in thulium is neglected and the resulting lifetime (38) is assumed constant. To determine whether these are reasonable approximations, the values of several spectroscopic parameters are required.

As discussed earlier, η_3 is likely to be close to zero. The value of β_{75} is not known, but is probably close to zero due to the ~50-μs multiphonon lifetime of the $7 \rightarrow 6$ transition in YAG [12]. To calculate the value of η_8, the values of τ_8, k_{8656}, and k_{8612} are needed. A value of the latter parameter has to our knowledge not been published. If this parameter is set equal to zero, $\eta_8 = 0.07$, based on measurements of the other two parameters in Ho:YAG [12]. As is shown in Tables I and III, published values of the UC constant k_{2168} in 6% Tm, 0.5% Ho:YAG are significantly larger than those of $k_{\Sigma\mathrm{Tm}}$ in 6% Tm:YAG. We may therefore, as a good approximation, neglect the UC losses that stem from the UC process in thulium. Owing to the large interval of published values of the UC rate, we have chosen to use $\eta_8 = 0$ in simulations in the rest of this work. In Table II, parameter values used in the simulations are listed.

The resulting lifetime in the thulium–holmium system is close to 10 ms in YAG. From (36), it can be found that the spontaneous decay rates and the UC loss rate are of the same size when $N_x/N_{\mathrm{Tm}} \approx 0.01$. Typically, this ratio is 0.05–0.10 in a CW Tm:Ho:YAG laser, indicating that UC is the dominant loss mechanism. Additionally, calculations of τ from (34) and (38) show that τ varies only slowly with N_x, depending on the ratio τ_2/τ_6. If this ratio is 2 (which is probably an overestimate) then the resulting lifetime τ is increased by 8% when N_x/N_{Tm} is increased from 0 to 0.1. Therefore, it can be considered as a good approximation to assume a constant τ, i.e., to use the small-signal values f_{Ho}^0 (35) when calculating τ from (38).

A. Interpretation of Published Values of k_{2168}

The published values of the UC parameter in Tm:Ho:YAG and Tm:Ho:YLF have been obtained with different theoretical approaches and can in some cases not be directly compared, although they commonly are. The differences stem from the rate-equation approach and how the UC losses are described, i.e., whether the decay of the upconverted populations back into the upper laser levels is accounted for and whether the thulium $^3F_4$ level and the holmium $^5I_7$ level are treated with different rate equations or a combined rate equation. The latter diversity can lead to a factor-of-two difference in the UC parameter since the UC term in most cases is expressed in the form $k \cdot N^2$, regardless of whether an UC event leads to a loss of one or two excitations in the upconverting level(s). If all the upconverted population decays back into the upper levels, the observed UC loss rate will be half of the actual UC rate since one UC event in this case leads to a net loss of only one ion in the upper level. This may then lead to a factor-of-two difference in the measured parameters. From (37), we see that one UC event leads to a loss of $(1 - \eta_8)(2 - \beta_8)$ excitations if η_3 and β_{75} are set equal to zero. In the literature, cross-relaxation from level 8 is commonly neglected ($\eta_8 = 0$). The net loss of excitations in a UC event then is $2 - \beta_8$.

Fan *et al.* [19] used a combined rate equation for the thulium and holmium upper levels and accounted for the decay back into the upper levels by assuming $\beta_8 = 1$. This approach was also used by Kintz *et al.* [30] and by Hansson *et al.* [31] in Tm:Ho:YLF. Bowman *et al.* [21] measured the total loss from UC and converted the measured loss to Fan's UC-parameter q. Bowman's loss-parameter Q is equal to the parameter $k_{\Sigma\mathrm{Ho}}$ introduced here, and Fan's UC-parameter q relates to the UC parameter in this work according to

$$k_{\Sigma\mathrm{Ho}} = \frac{f_{\mathrm{Ho}}(1 - f_{\mathrm{Ho}})}{2} q. \tag{39}$$

Antipenko *et al.* [32] and Nikitichev [25] have also used rate equations for the combined levels, but did not account specifically for decay of upconverted populations (equivalent to assuming $\beta_8 = 0$). Their measured values are therefore half of what they would have been in the approach of Fan, and they relate to the UC parameter $k_{\Sigma\mathrm{Ho}}$ as in (39), but where the right-hand side of the equation is multiplied with a factor-of-two. Dinndorf [33] used separate rate equations for thulium and holmium and accounted for the upconverted population by using rate equations for all interesting levels. His UC-parameter α_2 in Tm:Ho:YLF is equal to the k_{2168} used in this work. Shaw *et al.* [12] regarded UC in singly doped Ho:YAG and included the factor-of-two in front of the UC term in the

rate equation. He accounted for the UC population by using rate equations for all levels of interest. His measured values are equal to the UC parameters k_{6567} and k_{6568} in this work.

Additionally, Antipenko *et al.* [32] and Nikitichev [25] found the UC parameter in Tm:Ho:YAG to depend linearly on the thulium concentration for thulium concentrations 0–14% and to be independent of the holmium concentration for holmium concentrations 0–2%. Kintz *et al.* [30] found indications on a linear dependency between the UC parameter and the product of the thulium and holmium dopant concentrations. In Table III, published measurements of the UC parameters in 6% Tm, 0.5% Ho:YAG and 6% Tm, 0.5% Ho:YLF are listed and converted to parameters used in this work.

B. CW Operation

In steady-state operation, a fourth-degree equation for N_x is obtained when (34) is inserted into (36). This can be solved if the thulium UC processes are neglected and the resulting lifetime is assumed constant, which was justified above. We then obtain for the saturated upper level population density (40), shown at the bottom of the page, where we have defined

$$\begin{aligned} a_1 &= \frac{1+r_{\mathrm{HT}}\theta}{2(\theta-1)} & P_1 &= i_r - I_R + \kappa_{\mathrm{Ho}} a_1 \\ a_2 &= \frac{1-r_{\mathrm{HT}}\theta}{2(\theta-1)} & P_2 &= \frac{2+i_r+I_R-\kappa_{\mathrm{Ho}} a_2}{2} \\ a_3 &= \mathrm{sign}(P_1) & P_3 &= (1+a1i)i_r + (fr_{\mathrm{HT}} - a_1) I_R + \kappa_{\mathrm{Ho}} a_1^2 \end{aligned} \tag{41}$$

where $\mathrm{sign}(x) = +1$ or -1 when x is positive or negative, respectively. The dimensionless UC parameter, k_{Ho}, has been defined as

$$\kappa_{\mathrm{Ho}} = 2N_{\mathrm{Tm}}\tau(1-\eta_8)(2-\eta_8-\eta_7\beta_{87}(\beta_{75}+\eta_3))k_{2168} \tag{42}$$

where $k_{\Sigma\mathrm{Tm}}$ has been neglected in the deduction of (40). Here, i_r is the pump intensity relative to the thulium pump saturation intensity (20) and I_R is the laser intensity relative to a saturation intensity similar to (18), where all parameters inserted are holmium parameters $(\sigma, f_u, f_l, h\nu_L)$ except for τ_2 where the combined upper level lifetime τ is inserted [calculated with constant f_{Ho} from (35)]. These are not the true saturation intensities in the thulium–holmium system, but we have still chosen to use them for simplicity. (The true saturation intensities depend on f_{Ho} and thereby on N_x.) The holmium population density can then be calculated from (40) and (34), and the CW-laser output can be calculated in the same manner as for the CW thulium laser by use of (3).

In Fig. 6, results from simulations with (3), (34), and (40) are compared with simulations where UC and GSD are neglected for an end-pumped CW laser geometry. We see that there is a dramatic difference in predicted threshold pump power and that the predicted slope efficiency is reduced in our approach. The UC losses are the main reason for the higher threshold, while the GSD of thulium causes a reduced pump absorption efficiency and thereby a lower slope efficiency.

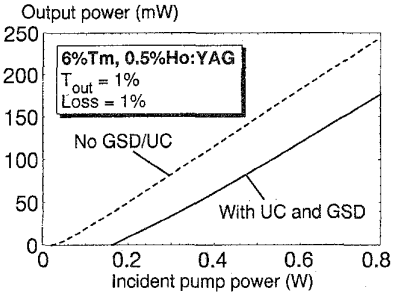

Fig. 6. Comparison of simulations of the CW Tm:Ho:YAG laser with different methods. Dashed line: Neglecting UC and GSD in both thulium and holmium. Solid line: Including UC and GSD, using (40) with $k^0_{\Sigma\mathrm{Ho}} = 20{\cdot}10^{-18}$ cm^3/s, where $k^0_{\Sigma\mathrm{Ho}}$ refers to the value of $k_{\Sigma\mathrm{Ho}}$ when $N_6 = 0$. Non-divergent pump and resonator modes were assumed, both with a Gaussian transverse distribution with 60-μm beam radius.

C. Q-Switched Operation

Q-switched operation in the thulium–holmium system is a bit more complex. We shall here be concerned with calculation of the population inversion density at the end of the pump pulse. The calculated population inversion distribution can then be used to simulate Q-switched operation.

The rate equation (36) cannot be solved by analytical means and needs numerical integration. However, if f_{Ho} can be assumed constant during the pump period, i.e., depletion of the holmium ground state can be neglected, then the system can be solved to yield results similar to those for the thulium system

$$\frac{N_x(t)}{N_{\mathrm{Tm}}} = \left\{ s_H \cdot \tanh\left(\frac{s_H t}{2\tau} + \mathrm{arctanh}\left(\frac{1+(1-f^0_{\mathrm{Ho}})i_r}{s_H} \right) \right) - \left(1+(1-f^0_{\mathrm{Ho}})i_r\right) \right\} / \kappa^0_{\Sigma Ho} \tag{43}$$

where s_H is given by

$$s_H = \sqrt{\left(1+(1-f^0_{\mathrm{Ho}})i_r\right)^2 + 2\kappa^0_{\Sigma\mathrm{Ho}} i_r} \tag{44}$$

and

$$\kappa^0_{\Sigma\mathrm{Ho}} = 2N_{\mathrm{Tm}}\tau k_{\Sigma\mathrm{Ho}} \tag{45}$$

is calculated with f^0_{Ho}. We have here used the nominal pump and laser saturation intensities, like for CW operation. In Fig. 7, the holmium upper laser level population density is plotted from (43) and compared with a numerical solution of (34) and (36) as a function of time and as a function of pump intensity. We see that the error of keeping f_{Ho} constant is small in this case.

$$\frac{N_x}{N_{\mathrm{Tm}}} = 0.5\left(a_3\sqrt{\left(a_2P_1^2+2P_2P_3\right)^2 - \left(P_1^2-4P_2^2\right)\left((a_1P_1)^2-P_3^2\right)} - \left(a_2P_1^2+2P_2P_3\right)\right) / \left((P_1/2)^2-P_2^2\right) \tag{40}$$

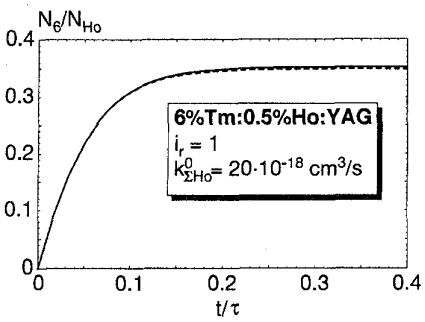

Fig. 7. Comparison of calculations of the relative upper level population in holmium as function of time when exposed to a constant pump intensity. Solid line: Numerical simulation of (36). Dashed line: Calculations based on (43). The time scale is normalized to the combined upper level lifetime.

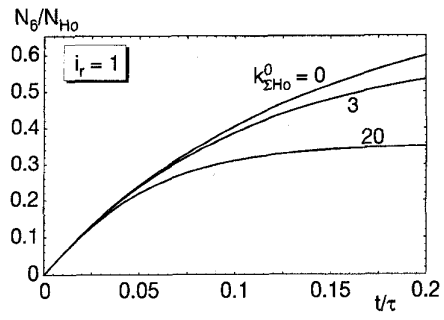

Fig. 8. Comparison of the temporal behavior of the upper laser level in holmium during pumping (without lasing) for various values of the UC parameter $k^0_{\Sigma \mathrm{Ho}}$ in units of 10^{-18} cm^3/s.

In Fig. 8, the effect of UC is shown for various values of $k_{\Sigma Ho}$ that span the range of published values. We see that UC losses severely limit the population inversion that can be stored in Tm:Ho:YAG, which limits the usability of this material in Q-switched operation. As listed in Table III, the reported values of k_{2168} in Tm:Ho:YLF are significantly lower, which makes this material somewhat better suited for pulsed operation. UC parameters for other thulium–holmium-doped materials have, to our knowledge, not been published.

V. Thermal Effects

The performance of thulium and holmium lasers depend strongly on the temperature of the laser material. A detailed study of the heat generation and temperature effects in these lasers requires accurate accounting for the different heat loads and cooling. In this section, a summary of the heat effects and the most important heat-generation mechanisms in the thulium–holmium system is given.

A. Effects of Temperature Changes

A temperature increase will lead to a change in the population distribution within an energy manifold in such a way that the lower Stark levels will be less populated and the higher levels will be more populated. This will have impact the laser performance in several ways. The lower laser level in a quasi-three-level laser is usually among the higher levels in the ground-state manifold, while the upper laser level is among the lower Stark levels in its energy manifold. A temperature increase will therefore have a negative effect on the gain through both the upper and lower laser level populations. This is observed as an increased pump threshold at higher temperatures, which leads to a reduced laser output for a given pump power.

The pump transition normally includes one of the lower levels in the ground-state manifold. Therefore, the pump absorption efficiency and thereby the laser efficiency will be reduced at higher temperatures. In the thulium–holmium system, the equilibrium between the $^3\mathrm{F}_4$ and $^5\mathrm{I}_7$ levels will be displaced toward the thulium $^3\mathrm{F}_4$ level (reduced θ and f_{Ho}) at higher temperatures, further reducing the gain (and possible energy extraction in Q-switched operation) in these systems.

The rates for nonradiative decay increase with increasing temperature [34]. It is also likely that the rates for nonresonant energy transfer will increase at higher temperatures. It is difficult to estimate the net effect of temperature changes on these processes, both since the exact temperature dependence is not well known and since increased energy transfer rates may have both positive (e.g., cross-relaxation) and negative (e.g., UC) effects on the laser performance.

The luminescence bandwidths tend to increase with increasing temperature [35]. Therefore, one may expect the stimulated emission cross section and the absorption cross section to be reduced at higher temperatures, which would both have a negative effect on the laser performance. Besides the effects on the atomic processes, the heat generation may lead to thermal lensing and stress-induced birefringence in the host materials, which can result in a reduced output from the laser and a reduced beam quality.

B. Sources of Heat Generation

The laser crystal is heated by the excitation of lattice vibrations (phonons) which are created through nonradiative decay, and created or annihilated to conserve the energy in energy transfer processes. Several processes contribute to the heat load in the thulium and holmium lasers. The energy difference between the pump photon and the laser photons is 20–25% of the pump photon energy in these materials, representing the minimum heat load. The nonradiative decay following the UC processes is another major heat source. Of the UC processes in thulium, each UC event to level 4 will lead to a heat load of

$$Q_4 \approx (1-\eta_4-\beta_{43}\eta_3)(\beta_{42}(1-\zeta_{42})\varepsilon_{42} + \beta_{43}(1-\zeta_{43})\varepsilon_{43} + \beta_{43}\beta_{32}(1-\zeta_{32})\varepsilon_{32}) \quad (46)$$

where ζ_{ij} is the ratio of the radiative to the total decay rate of the $i \rightarrow j$ transition, and ε_{ij} is the energy of this transition. The first factor is the fraction of ions that do not decay from level 4 to level 2 through cross-relaxation. The last factor consists of three terms, accounting for direct (first term) and indirect spontaneous decay from level 4 to level 2. Using parameter values listed in Table II together with $\zeta_{42} = 1$ and $\zeta_{32} = 0$ [10], we find $Q_4 \approx \beta_{43}(1-\eta_4)(h\nu_L - \zeta_{43}\varepsilon_{43})$, where $h\nu_L$ is the laser photon energy. If we further insert $\eta_4 = 0.97$

(Table II), $\beta_{43} = 0.5$, and $\zeta_{43} = 0.05$ [10], we find that $Q_4 \approx 0.01 h\nu_L$. Each UC event to level 3 will result in a heat load $Q_3 \approx (1-\eta_3)h\nu_L$. The heat load per UC event to level 4 is then significantly smaller than for UC to level 3. As can be seen from Table I, the UC rates to level 3 and 4 in Tm:YAG are approximately equal. Therefore, the UC to level 3 is the dominant heat source, resulting from UC in thulium.

In the holmium system, the heat load from the cooperative UC process to level 8 can be approximated by

$$Q_8 \approx (1-\eta_8)\beta_{87}(\varepsilon_{87}+\eta_7\varepsilon_{72}+(1-\eta_7)\beta_{76}(1-\zeta_{76})\varepsilon_{76}) \quad (47)$$

where cross-relaxation from level 7 has been ignored, and $\beta_{32} = 1$, $\zeta_{32} = 0$, and $\zeta_{87} = 0$ have been assumed. The factor $(1-\eta_8)\beta_{87}$ is the fraction of ions excited to level 8 that decay to level 7. In the second factor, the second term accounts for nonradiative decay back to level 2 through energy transfer to thulium, and the last term accounts for nonradiative decay back to level 6 in holmium. Assuming $\beta_{87} = 1$, $\beta_{76} = 1$, and $\zeta_{76} = 0$, we find that $Q_8 \approx (1-\eta_8)h\nu_L$. This indicates that the heating from UC is larger in Tm:Ho:YAG than in Tm:YAG due to the significantly higher UC rates.

A full simulation of the laser accounting for the variety of thermal effects discussed above has not been within the scope of this work. Such a simulation would need to take into account the detailed distribution of the pump laser light, the details of the cooling geometry, and the temperature dependence of both the heat generation rates and the gain distribution. Inclusion of thermal effects in the simulations will be particularly important in the design of high-power systems, and it is a subject of continued interest at our lab.

VI. Comparison with Experimental Results

A standard CW end-pumped laser was studied. The resonator consisted of a flat dichroic mirror that transmitted the pump light and was highly reflective at 2 μm, and a 5-cm radius of curvature 1% output coupler. The pump light was tightly focused inside the laser material with a beam radius of about 60 μm inside the laser rod. The laser rod was placed close to the flat dichroic mirror and the resonator length was adjusted to obtain maximum laser output power for a given pump power. This is obtained when the resonator mode is matched to the pump mode. The laser rods used were 6% Tm:YAG, 6% Tm, 0.5% Ho:YAG, and 6% Tm, 0.5% Ho:YLF, and all rods were 5 mm long. The pump source was a tunable CW titanium–sapphire laser delivering up to 0.8 W of pump power, which was tuned to maximum absorption in the laser materials (~785 nm in YAG and ~792 nm in YLF). At the absorption peak, approximately 94% of the pump radiation was absorbed in the rod at small pump signal levels. All lasers oscillated in the fundamental transverse mode and in a number of longitudinal modes centered at 2015 nm in Tm:YAG, 2053 nm in Tm:Ho:YLF, and 2096 nm in Tm:Ho:YAG.

The laser performance was simulated according to (3), (16), and (40), where the beams were assumed to have the observed fundamental Gaussian transverse profile. The round-trip losses were varied to fit the calculated slope efficiency

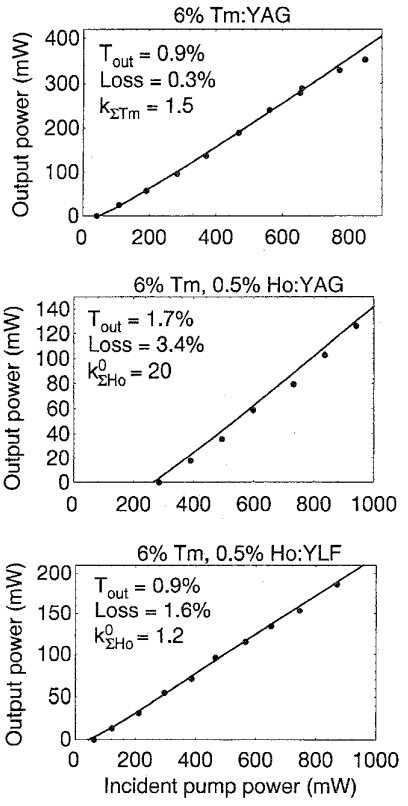

Fig. 9. Comparison of experimental results and numerical simulations based on (3), (16), and (40). $k_{\Sigma Tm}$ and $k_{\Sigma Ho}$ are given in units of 10^{-18} cm^3/s.

to the experimental slope efficiency, and the UC constants were varied to fit the threshold value. The differences in round-trip losses probably stem from a poorer AR coating on the codoped rods, which were AR-coated in-house, while the Tm:YAG rod was coated by the rod manufacturer. The best-fit UC constants were within the range of published values. The simulations based on the theory derived in this paper were in general in good agreement with the experimental results. The experimental results and numerical simulations are compared in Fig. 9.

The considerably higher threshold that was observed in Tm:Ho:YAG than in Tm:YAG can be explained with the much higher UC rate in Tm:Ho:YAG and the higher internal losses. The simulations showed that improved AR-coatings on the Tm:Ho:YAG rod would slightly reduce the threshold pump power; from 265 mW to 205 mW (the latter value calculated with the same loss and mirror transmission as for Tm:YAG). However, the most important contribution to the higher threshold value stems from the UC losses. If the value of the UC parameter was reduced from $k_{2168} = 80 \cdot 10^{-18}$ cm^3/s, which was used in Fig. 9 and is in the high range of published values (see Table III), to the low-range value $k_{2168} = 12 \cdot 10^{-18}$ cm^3/s, then the predicted threshold pump power was reduced from 265 mW to 75 mW. This illustrates the importance of the UC processes in the thulium–holmium-doped laser and suggests that the UC parameter may be determined from laser threshold measurements.

VII. Conclusion

We have developed a mathematical description of a laser-pumped quasi-three-level laser, where the spatial distributions of the pump and resonator modes have been accounted for. The model was specialized to thulium- and thulium–holmium-doped lasers, and special attention was given to include the effects of different UC loss processes in thulium and holmium, as well as the depletion of the ground states at high inversion levels. Simulations with the developed models showed that these effects may be important both in CW and Q-switched laser operation. In particular, we saw that the UC losses in Tm:Ho:YAG lasers can significantly reduce the output from the laser. However, the published values of the UC parameter in Tm:Ho:YAG span a large range and, consequently, there are considerable uncertainties in simulations of these laser systems.

Results from experiments with end-pumped thulium- and thulium–holmium-doped lasers were compared with results from numerical simulations. The UC parameters used in the numerical simulations were varied to fit the calculated threshold pump power to the experimental results. Good agreement between experiment and simulations were obtained for UC parameters within the range of published values.

References

[1] B. M. Antipenko, S. P. Voronin, V. F. Maïboroda, and T. A. Privalova, "Influence of summation of excitations on the efficiency of lasing of sensitized media," *Sov. J. Quantum Electron.*, vol. 16, pp. 640–644, 1986.

[2] K. H. Kim, Y. S. Choi, R. V. Hess, C. H. Blair, P. Brockman, N. P. Barnes, G. W. Henderson, and M. R. Kokta, "Experiments and theory for a Tm:Ho:YAG laser end pumped by a Cr:GSAG laser," *OSA Proc. Adv. Solid State Lasers*, H. P. Jenssen and G. Dubé, Eds. Washington, DC: Opt. Soc. Amer., 1990, vol. 6, pp. 155–161.

[3] R. R. Petrin, M. G. Jani, R. C. Powell, and M. Kokta, "Spectral dynamics of laser-pumped $Y_3Al_5O_{12}$:Tm,Ho lasers," *Opt. Mater.*, vol. 1, pp. 111–124, 1992.

[4] T. Y. Fan and R. Byer, "Modeling and CW operation of a quasithree-level 946 nm Nd:YAG laser," *IEEE J. Quantum Electron.*, vol. 23, pp. 605–612, 1987.

[5] W. P. Risk, "Modeling of longitudinally pumped solid-state lasers exhibiting reabsorption losses," *J. Opt. Soc. Amer.*, vol. B5, pp. 1412–1423, 1988.

[6] P. F. Moulton, "An investigation of the Co:MgF_2 laser system," *IEEE J. Quantum Electron.*, vol. 21, pp. 1582–1595, 1985.

[7] A. Siegman, *Lasers*. Mill Valley, CA: Univ. Sci. Books, 1986.

[8] G. Armagan, A. M. Buoncristiani, A. T. Inge, and B. DiBartolo, "Comparison of spectroscopic properties of Tm and Ho in YAG and YLF crystals," *OSA Proc. Adv. Solid State Lasers*, G. Dubé and L. L. Chase, Eds. Washington, DC: Opt. Soc. Amer., 1991, vol. 10, pp. 222–226.

[9] T. Becker, R. Clausen, G. Huber, E. W. Duczynski, and P. Mitzscerlich, "Spectroscopic and laser properties of Tm-doped YAG at 2 μm," *OSA Proc. Tunable Solid State Lasers*, M. L. Shand and H. P. Jenssen, Eds. Washington, DC: Opt. Soc. Amer., 1989, vol. 5, pp. 150–153.

[10] J. A. Caird, L. G. DeShazer, and J. Nella, "Characteristics of room-temperature 2.3-μm laser emission for Tm^{3+} in YAG and $YAlO_3$," *IEEE J. Quantum Electron.*, vol. 11, pp. 874–881, 1975.

[11] J. B. Gruber, M. E. Hills, R. M. MacFarlane, C. A. Morrison, G. A. Turner, G. J. Quarles, G. J. Kintz, and L. Esterowitz, "Spectra and energy levels of Tm^{3+}:$Y_3Al_5O_{12}$," *Phys. Rev. B.*, vol. 40, pp. 9464–9478, 1989.

[12] L. B. Shaw, R. S. F. Chang, and N. Djeu, "Measurement of up-conversion energy-transfer probabilitites in Ho:$Y_3Al_5O_{12}$ and Tm:$Y_3Al_5O_{12}$," *Phys. Rev. B.*, vol. 50, pp. 6609–6619, 1994.

[13] G. Armagan, B. M. Walsh, N. P. Barnes, A. M. Buoncristiani, and E. A. Modlin, "Determination of Tm-Ho rate coefficients from spectroscopic measurements," *OSA Proc. Adv. Solid State Lasers*, T. Y. Fan and B. Chai, Eds. Washington, DC: Opt. Soc. Amer., 1994, vol. 20, pp. 141–145.

[14] S. R. Bowman, G. J. Quarles, and B. J. Feldman, "Upconversion losses in flashlamp-pumped Cr, Tm:YAG," *OSA Proc. Adv. Solid State Lasers*, L. L. Chase and A. A. Pinto, Eds. Washington, DC: Opt. Soc. Amer., 1992, vol. 13, pp. 169–173.

[15] G. J. Kintz, "Highly efficient CW 2-μm laser," presented at the *OSA Annu. Meet.*, 1990.

[16] G. Rustad, "Modeling and experimental investigation of laser-diode end-pumped and side-pumped thulium- and holmium doped lasers," Dr. Scient. dissertation, University of Oslo, Oslo, Norway, 1994.

[17] H. Ajer, S. Landrø, and K. Stenersen, "Numerical simulations of diode side-pumped Q-switched Nd:YAG oscillators and amplifiers with rod and zig-zag slab crystal geometry," *OSA Proc. Adv. Solid State Lasers*, T. Y. Fan and B. H. T. Chai, Eds. Washington, DC: Opti. Soc. Amer., 1994, vol. 20, pp. 20–24.

[18] G. Rustad, H. Hovland, and K. Stenersen, "Low threshold laser-diode side pumped Tm- and Tm:Ho lasers," *Conf. Lasers and Electro-Opt.* (OSA Tech. Dig. Ser.). Washington, DC: Opt. Soc. Amer., vol. 8, paper CThL5, 1994.

[19] T. Y. Fan, G. Huber, R. L. Byer, and P. Mitzscherlich, "Spectroscopy and diode laser-pumped operation of Tm, Ho:YAG," *IEEE J. Quantum Electron.*, vol. 24, pp. 924–933, 1988.

[20] D. L. Dexter, "A theory of sensitized luminescence in solids," *J. Chem. Phys.*, vol. 21, pp. 836–850, 1953.

[21] S. R. Bowman, M. J. Winings, R. C. Y. Auyeung, J. E. Tucker, S. K. Searles, and B. J. Feldman, "Laser and spectral properties of Cr, Tm, Ho:YAG at 2.1 μm," *IEEE J. Quantum Electron.*, vol. 27, pp. 2142–2149, 1991.

[22] V. A. French, R. R. Petrin, R. C. Powell, and M. Kokta, "Energy-transfer processes in $Y_3Al_5O_{12}$:Tm, Ho," *Phys. Rev. B*, vol. 46, pp. 8018–8026, 1992.

[23] B. T. McGuckin, R. T. Menzies, and H. Hemmati, "Efficient energy extraction from a diode-pumped Q-switched Tm, Ho:$YLiF_4$ laser," *Appl. Phys. Lett.*, vol. 59, pp. 2926–2928, 1991.

[24] D. E. Castleberry, "Energy transfer in sensitized rare earth lasers," Ph.D. dissertation, Massachusetts Inst. of Technol., Cambridge, 1975.

[25] A. A. Nikitichev, "Temperature dependence of the gain in $Y_3Al_5O_{12}$:Cr^{3+}:Tm^{3+}:Ho^{3+}," *Sov. J. Quantum Electron.*, vol. 18, pp. 918–919, 1988.

[26] K. M. Dinndorf and H. P. Jenssen, "Distribution of stored energy in the excited manifolds of Tm and Ho in 2 micron laser materials.," *OSA Proc. Adv. Solid State Lasers*, T. Y. Fan and B. H. Chai, Eds. Washington, DC: Opt. Soc. Amer., 1994, vol. 20, pp. 131–135.

[27] J. B. Gruber, M. E. Hills, M. D. Seltzer, S. B. Stevens, C. A. Morrison, G. A. Turner, and M. R. Kokta, "Energy levels and crystal quantum states of trivalent holmium in yttrium aluminum garnet," *J. Appl. Phys.*, vol. 69, pp. 8183–8204, 1991.

[28] H. P. Jenssen, A. Linz, R. P. Leavitt, C. A. Morrison, and D. E. Wortman, "Analysis of the optical spectrum of Tm^{3+} in $LiYF_4$," *Phys. Rev. B.*, vol. 11, pp. 92–101, 1975.

[29] N. Karyianis, D. E. Wortman, and H. P. Jenssen, "Analysis of the optical spectrum of Ho^{3+} in $LiYF_4$," *J. Phys. Chem. Solids*, vol. 37, pp. 675–682, 1976.

[30] G. Kintz, I. D. Abella, and L. Esterowitz, "Upconversion coefficient measurement in Tm^{3+}, Ho^{3+}:YAG at room temperature," in *Proc. Intl. Conference on Lasers'87*, F. J. Duarte, Ed. McLean, VA: STS, 1988, pp. 398–403.

[31] G. Hansson, A. Callenås, and C. Nelsson, "Upconversion studies in laser diode pumped Tm, Ho:$YLiF_4$," *OSA Proc. Adv. Solid State Lasers*, A. A. Pinto and T. Y. Fan, Eds. Washington, DC: Opt. Soc. Amer., 1993, vol. 15, pp. 446–449.

[32] B. M. Antipenko, V. A. Buchenkov, A. S. Glebov, T. I. Kisleva, A. A. Nikitchev, and V. A. Pismennyi, "Spectroscopy of YAG:CrTmHo laser crystals," *Opt. Spectrosc. (USSR)*, vol. 64, pp. 772–774, 1988.

[33] K. M. Dinndorf, "Energy transfer between thulium and holmium in laser hosts," Ph.D. dissertation, Massachusetts Inst. Technol., Cambridge, 1993.

[34] L. A. Riseberg and H. W. Moos, "Multiphonon orbit-lattice relaxation of excited states of rare-earth ions in crystals," *Phys. Rev.*, vol. 174, pp. 429–438, 1968.

[35] A. A. Kaminskii, "Laser crystals," D. L. MacAdam, Ed., *Springer Series in Optical Sciences*. New York: Springer Verlag, 1981, vol. 14.

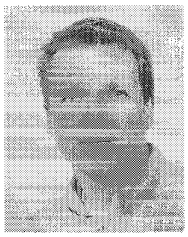

Gunnar Rustad was born in Hedalen, Norway, on April 3, 1966. He received the Sivilingeniør degree in physics from the Norwegian Institute of Technology, Trondheim, in 1990 and the Dr. Scient degree in physics from the University of Oslo, Norway, in 1995.

Since 1990, he has been with the Norwegian Defence Research Establishment, Kjeller, where he has worked with diode-pumped solid-state lasers. His thesis research concentrated on the spectroscopy and design of thulium- and holmium-doped lasers. His current research interests include development of diode-pumped solid-state lasers and use of nonlinear frequency conversion techniques.

Knut Stenersen was born in Kvam, Norway, in 1952. He received the Sivilingeniør degree in physics from the Norwegian Institute of Technology, Trondheim, in 1977 and the Dr. Scient. degree in physics from the University of Oslo, Norway, in 1982.

Since 1977, he has been employed at the Norwegian Defence Research Establishment, Kjeller, where, he has worked on research and development in the fields of high-pressure continuously tunable CO_2 and N_2O lasers, mode-locked lasers, atmospheric spectroscopy, atmospheric laser communication systems, tunable solid-state lasers, diode-pumped solid-state lasers, and nonlinear frequency conversion techniques. From 1983 to 1984, he was a Visiting Scientist at the Hughes Research Laboratories, Malibu, CA, where he worked with phase conjugation, picosecond optoelectronics, and nonlinear parametric processes in optical fibers.